




Article

Convective Bubbly Flow of Water in an Annular Pipe: Role of Total Dissolved Solids on Heat Transfer Characteristics and Bubble Formation

M. M. Sarafraz ¹, M. S. Shadloo ², Zhe Tian ³, Iskander Tlili ⁴, Tawfeeq Abdullah Alkanhal ⁵, Mohammad Reza Safaei ^{6,7,*}, Marjan Goodarzi ⁸ and M. Arjomandi ¹

¹ School of Mechanical Engineering, The University of Adelaide, Adelaide, SA 5005, Australia

² CORIA-UMR 6614, Normandie University, CNRS-University & INSA, 76000 Rouen, France

³ School of Engineering, Ocean University of China, Qingdao 266100, China

⁴ Department of Mechanical and Industrial Engineering, College of Engineering, Majmaah University, Al-Majmaah 11952, Saudi Arabia

⁵ Department of Mechatronics and System Engineering, College of Engineering, Majmaah University, Al-Majmaah 11952, Saudi Arabia

⁶ Division of Computational Physics, Institute for Computational Science, Ton Duc Thang University, Ho Chi Minh City, Vietnam

⁷ Faculty of Electrical and Electronics Engineering, Ton Duc Thang University, Ho Chi Minh City, Vietnam

⁸ Department of Mechanical Engineering, Lamar University, Beaumont, TX 77705, USA

* Correspondence: cfd_safaei@tdtu.edu.vn; Tel.: +1-502-657-9981

Received: 28 June 2019; Accepted: 24 July 2019; Published: 29 July 2019



Abstract: Formation of bubbles in water inside an annulus pipe in a flow boiling regime was experimentally investigated. The effect of various variables, such as total dissolved solid materials (TDS) in terms of mass fraction, flow rate of water, and applied heat flux (HF) on the heat transfer coefficient (HTC) and bubble behavior of water, was experimentally investigated. A regression formula was fitted to estimate the average bubble diameter at various TDS values, with accuracy of <4.1% up to heat flux of 90 kW/m². Results show that the presence of TDS materials can increase the contact angle of bubble and bubble diameter, and also promotes the HTC value of the system. However, flow rate of water suppressed bubble generation, and increased the heat transfer coefficient due to the renewal of the thermal boundary layer around the boiling surface. Likewise, it was identified that forced convective and nucleate boiling heat transfer mechanisms contribute to the flow of boiling water, and heat flux is a key parameter in determining the mechanism of heat transfer. In the present study, heat flux of 15 kW/m² at 50 °C was the heat flux in which onset of nucleate boiling was identified inside the annulus pipe. The contact angle of water at TDS values of 300 mg/L and 1200 mg/L was 74° and 124°, respectively, showing the improvement in heat transfer characteristics of water due to the presence of TDS materials.

Keywords: contact angle; annulus pipe; bubble formation; radial heat flux; total dissolved solid material; convective flow

1. Introduction

Two-phase flow in pipes and annulus media is one of the most important flow regimes, with various applications in industrial sectors and domestic cooling/heating systems, which can be applied to mixtures of liquids and gases through pipes, channels, and industrial loops [1,2]. The dominant mechanism of heat transfer, which approximately occurs at isothermal condition is referred to as the “boiling and condensation” phenomenon [3], which has a larger heat transfer coefficient compared to

the conventional single-phase systems. Existence of such processes can cause significant improvement in thermal efficiency of the cycles [4]. Hence, convective flows are known to have a large heat transfer coefficient and great thermal performance over a small temperature difference [5].

Boiling heat transfer is the dominant mechanism in energy production sectors, waste heat boiler and in cooling industries and air conditioning, which perfectly vaporizes the working fluid [6–8]. During the boiling phenomenon, the micro-layer of the fluid close to the surface absorbs a large amount of heat, and the local vapor pressure of this micro-layer equals to the saturation pressure (or under a constant pressure, the temperature of the micro-layer becomes equivalent to the saturation temperature of the fluid). In this condition, the liquid uses the absorbed heat to supply the latent heat required for the phase change [9]. Likewise, the characteristics of the heating surface can strongly influence the boiling performance [10]. Parameters such as size distribution of the micro-cavities, the number of active nucleation position, the geometry of surface cavities, and the properties of solid-liquid interface can affect the bubble formation and the average size of the bubbles [11,12]. Such complexities are strong drivers for further research on bubbling and bubbly flow in different systems, including pipes and annulus media [13].

The formation of bubbles in pipes, and their interactions, can change the fluid dynamic and thermal behavior of the systems [14]. Generally, bubble movement augments the local turbulence and causes small micro-convective streams to form in the periphery of bubbles, and the thermal boundary layer is regenerated, which results in an increase in the heat transfer coefficient [15–17]. Convective flow boiling is a mechanism of boiling in which an external force circulates the working fluid around a heating surface. This case is vastly seen in industrial and domestic applications, from process plants to car cooling systems and central processor units (CPU) coolers in gaming computers [18,19]. In a flow boiling system, nucleate boiling and forced convection heat transfer are observed when the temperature of the surface and the heat flux applied to the surface are well above the saturation temperature of the working fluid [20]. These two mechanisms are separated from each other in a point referred to as onset of nucleate boiling (ONB).

The volume of bubbles in comparison with the amount of liquid determines various flow regimes, such as bubbly flow, slug flow, annular flow, transition flow, and mist flow [21,22]. Recognizing flow patterns and how bubbles form are necessary for figuring out the two-phase flow, thermal performance, and dynamic of the flow within the pipe or annulus [23–26]. Much effort has been made to understand the behavior of the bubbles in a convective bubbly flow. For example, Lahey and Ohkawa [27] investigated the flow patterns created in a vertical annular channel utilizing gamma ray to identify the gas holdup. Kelessidis and Dukler [28] mapped the flow patterns, which occurred in upward fluid flow in concentric and eccentric annulus. They used density function analysis of conductance probe signals. They found that the fluid flow could behave as bubbly, slug, annular as well annular with lumps, and churn. Osamasali and Chang [29] performed a series of experiments to recognize the flow pattern of a two-phase flow in three types of horizontal pipe with an inner diameter of 50.8 mm and outer diameters of 81.9, 101.6, and 135.4 mm. Flow patterns of smooth, plug, wavy, and annular varieties were detected in the experiments. Ekberg et al. [30] investigated various types of flow patterns in concentric pipes with lengths of 430 mm. Air with velocity between 0.02 and 57 m/s, and water between 0.1 and 6.1 m/s, were introduced to the pipes. They observed that the air could behave in water as slug/plug, annular/slug, stratified, stratified/slug, bubbly/plug, churn, and dispersed bubbly, resulting in better mixing and heat transfer. Thorncroft et al. [31] performed several experiments to understand the mechanism supporting the growth of bubbles through a boiling flow in a vertical pipe by means of a high-speed camera. They studied the bubble size and the rate of the bubble growth and found that the characteristics of bubbles in downflow boiling is considerably different from those recorded in the upflow boiling pipes. Bibeau and Salcudean [32] observed that the bubbles can grow over the hot surface until the rates of condensation and evaporation are the same and an equilibrium occurs on the boiling surface. Situ et al. [33] experimentally investigated the heat transfer characteristics of water under flow boiling inside a pipe. They performed their experiments in an annulus pipe with

upflow condition and utilized a high-speed camera to evaluate the bubble behavior inside the system. They found that at atmospheric pressure, the bubble departure frequency is dependent on heat flux rate close to the boiling surface. Chen et al. [34] studied subcooled flow boiling in a horizontal annular duct with two gaps at 1 and 2 mm. The results indicated that increasing the mass flux and the input of the subcooling cause bubbles to suppress and their density to decrease.

To achieve higher heat transfer and bubble formation in pool boiling, Gerardi et al. [35] utilized high-speed video and infrared thermometry to evaluate the bubble detachment from the boiling surface in a pipe, and identified the rate of bubble growth, bubble departure diameter, bubble holdup, and nucleation site density. Surgrue et al. [36] experimentally measured the influence of mass and heat flux, pressure (101 kPa to 505 kPa), orientation angle (0° to 180°), and subcooling (10 and 20°C) on the bubble dynamics in a pipe. To conduct the study, they used a high-speed video facility and an LED lighting method. The results indicate that by decreasing the mass flux, subcooling, and pressure, as well as increasing the heat flux, the average bubble departure diameter was increased. As can be seen, extensive studies have been conducted on the bubble formation of water inside different media. Table 1 summarizes the experimental condition and the results projected in some of the studies.

Table 1. Review of papers about bubble formation inside the pipes in flow boiling flow regime.

Author(s)	Year	Studied Liquid	Flow Conditions	Heat Flux (kW.m^2)	Results
Lazarek and Black [37]	1982	R-113	Saturated flow boiling in vertical tube	0.95–45	Heat transfer coefficient is not affected by local vapor qualities.
Jung et al. [38]	1989	Mixture of R22-R114	Flow boiling in horizontal annulus	1045	Suppressed nucleate boiling without considering the transition. Heat transfer coefficient of evaporation area is 36% lower than the other area.
Bao et al. [39]	2000	Freon R11 and HCFC123	Flow boiling in horizontal tube	5–200	Heat transfer coefficient affected by heat flux and pressure, but did not affect mass flux and the quality of vapor.
Yeoh and Tu [40]	2005	Water	Subcooled flow boiling	152.3 and 251.5	The model accurately predicts radial void fraction, bubble mean diameter, and velocity profile.
Chang and Ferng [41]	2019	Water	Saturated pool boiling	15.5–82.7	Increasing bubble departure frequency and temperature difference leads to bubble departure frequency and diameter augmentation. At low heat flux, isolated bubbles form and at high heat flux bubbles coalescence.
Wang et al. [42]	2019	Water and surfactant	Flow boiling in rectangular channel	290	Adding surfactant leads to bubble density, critical heat flux, and heat transfer coefficient increment. Coalescence of bubbles causes lack of effect in nucleation sites, so the heat transfer reduces.
Yin et al. [43]	2019	Water	Flow boiling in vertical tube	5–27.5	Tube height significantly affects flow temperature and phase distributions. First one, third of tube bubbly; second, one third cap; and last, one third churn flow patterns are observed. Boiling properties are identified by flow pattern and heat transfer regime interaction.
Eraghubi et al. [44]	2019	HFE7000	Flow boiling in vertical tube	8.8–61.7	After the beginning of the nucleate, bubbly flow pattern is observed. Slug flow pattern leads to heat transfer enhancement. Mass flux has no remarkable influence on the boiling curves; however, the transition of flow pattern is affected by it.

In light of the above-discussed studies, there is a need for further research on bubble formation in pipes. Bubbles can produce micro-convective streams and tensions, while renewing the thermal

and fluid dynamic boundary layers [45,46], which can cause some change in the behavior of the fluid. Moreover, the behavior of the bubbles depends strongly on the characteristics of the fluid, such as thermal conductivity and density. Total dissolved solid materials, referred to as TDS, can considerably change the physical and chemical properties of water, causing a change in the thermal and dynamic behaviors of water in pipes. To the best of the authors' knowledge, the effect of TDS material on the heat transfer coefficient (HTC) and bubble formation in annular flow has not been investigated in the literature. Hence, in the present work, a test rig is designed and fabricated to measure the heat transfer coefficient and bubble departure diameter in a flow boiling regime. The effect of mass concentration of solid materials, the mass flow rate and thermal flux, the bubble diameter of water, and the heat transfer coefficient at various TDS values are investigated and discussed. Using regression analysis, the bubble diameter was correlated against TDS value and heat flux. The results of this study can be used in heat exchanger designs and industrial plants which use water at different TDS values.

2. Experimental

2.1. Test Setup

In Figure 1, the test setup is shown, which has a main tank to contain the working fluid (here, water at different TDS values). The circulation system includes a centrifugal pump, a bypass loop, valves, an ultrasonic flow meter to constantly measure the flow rates of the fluid, and a cooling radiator to dissipate the heat and maintain the tank temperature at a constant value. Circulation of the fluid is done via a centrifugal pump within the system, and the inlet and outlet temperature of water before and after the test section was measured with two RTD thermometers mounted upstream and downstream of the considered section. To eliminate temperature overshoot, the tank temperature was controlled with a cooling radiator with an electric fan. The speed of the fan was controlled with a proportional–integral–derivative (PID) controller, such that when the outlet temperature of the test section exceeds a target value, the fan speed is increased to suppress the temperature overshoot. To record the pressure drop within the system, at the upstream and downstream part of the test section, pressure transmitters were placed to constantly report the pressure value to the data logger. The heart of the system is an annulus pipe, which includes a stainless steel rod placed inside a water pipe. The diameter of the annulus was 8 cm, while the diameter of the stainless steel rod was 2 cm. This was to ensure a laminar flow within the system. Hence, the effect of the turbulence can be minimized. Also, this geometrical specification provided a Reynolds number range from 397 to 1987 for $Q = 1$ L/min to 5 L/min in the laminar flow regime. A cartridge heater was placed inside the stainless steel rod to produce the radial thermal energy used for the bubble formation. The automatic transformer was connected to the cartridge heat to adjust the voltage and heat flux applied to the stainless steel rod. The body of the annulus was fabricated from Pyrex glass to enable visualization of the bubble formation phenomenon. Four k-type thermocouples were used to measure the stainless steel rod's surface temperature, which were installed close to the surface of the rod. All thermocouples, flow meters, and pressure sensors were connected to a data logger with a frequency of 1 kHz to log the data. The data logger was connected to a PC to record and process the data. Figure 1b shows the details of the rod, which was made of stainless steel.

To measure the bubble diameter, a high-speed camera (Casio EX-F1) was utilized and the images were processed in Matlab software using image processing tools to estimate the bubble diameter. To improve the quality of assessment, a contrast filter, together with sharpness effect, was utilized to clearly distinguish the border of the bubbles. The software and detailed information of the visualization technique has already been used and verified in our previous publication [47].

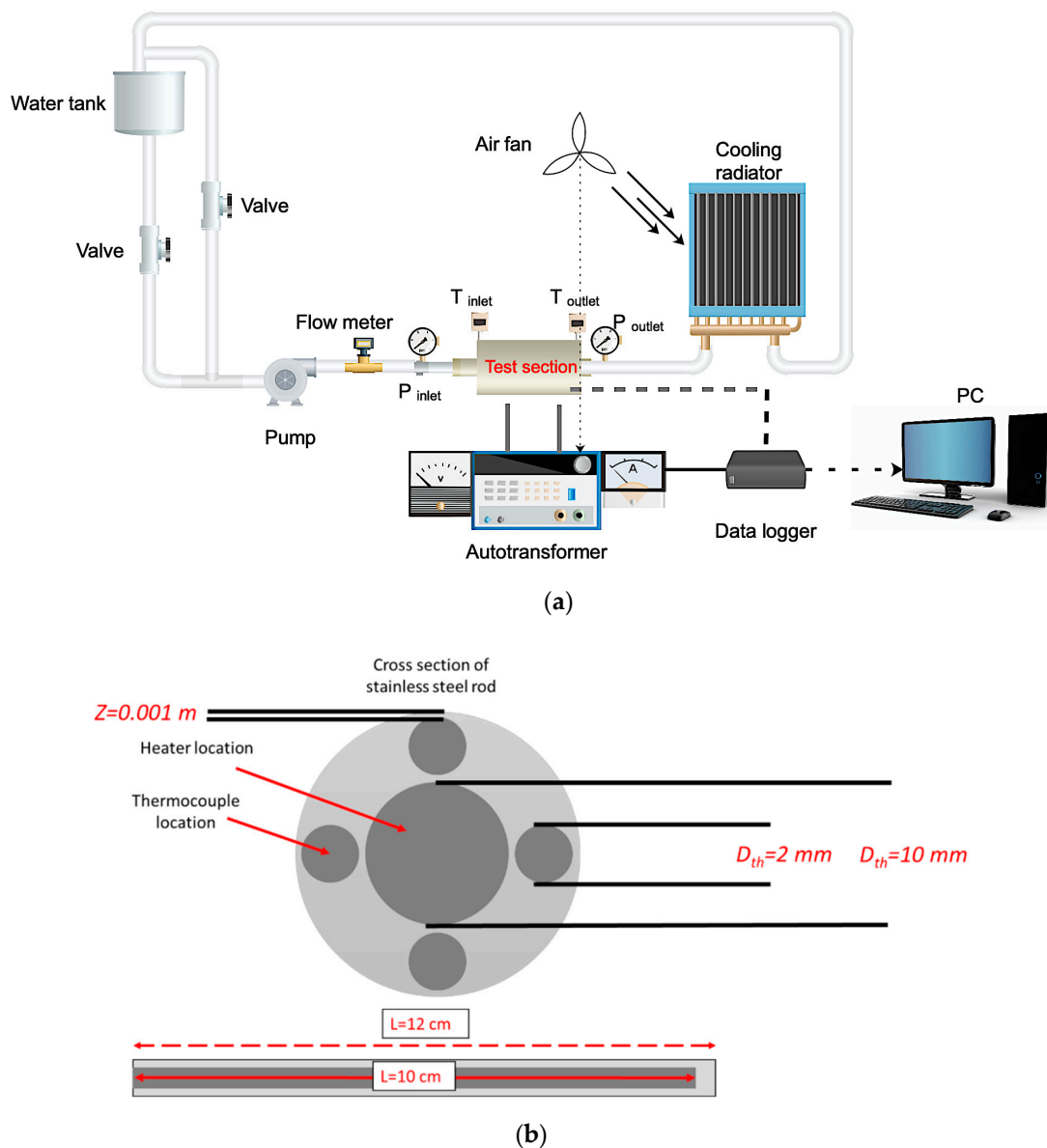


Figure 1. (a) Test setup and (b) detailed specifications of the stainless steel rod used as the heating surface.

2.2. Heat Loss Analysis and Analysis of Uncertainty

The heat flux is calculated with the following equation:

$$q'' = \frac{V \times I}{A}. \quad (1)$$

where I is the electric current measured with a digital multi-meter, V is the heater voltage, and A is the rod circumference area. Note that the stainless steel rod has a diameter equal to 2 cm. For calculating the heat transfer, the following formula was used [48–54]:

$$h = \frac{m \times C_p \times (T_{out} - T_{in})}{A \times (T_s - T_b)} \quad (2)$$

where m is the mass flow rate of water passing the annulus around the boiling surface, C_p is the heat capacity, T is the temperature, and indices *out*, *in*, *s*, and *b* stand for outlet, inlet, surface, and bulk section, respectively. The surface temperature was calculated as arithmetic average of the temperature

reading from the thermocouples. However, the temperature readings must be amended with Equation (3). Again, A is the circumference of the rod (heating surface) and h is the convective boiling heat transfer coefficient of the water. The thermocouples were not attached to the surface, and therefore, the thermal resistance between the thermocouple location and actual surface temperature was also estimated and the temperature readings were amended with the following equation:

$$T_s = T_{th} - \frac{q'' \times z}{k}. \quad (3)$$

where z is the small difference between the location of the thermocouples and the surface, th stands for the thermocouple, and k is the thermal conductivity of stainless steel (40 W/(mK)). To assess the potential loss of heat from the test setup, the following equation was used:

$$Q_{loss} = Q_{input} - Q_{absorbed \text{ by working fluid}} = V \times I - m \times C_p \times (T_{out} - T_{in}). \quad (4)$$

Figure 2 presents the value of the heat loss quantified at various heat fluxes. Only $\pm 5\%$ of total energy input to the system was lost, based on the figure. It was also identified that heat loss was higher at larger heat fluxes. Hence, the system (except for the Pyrex section) was heavily insulated with glass wool to minimize the heat loss to environment. It was also identified that the casing of the pump, together with the valves, were the main sources of heat loss, which were further insulated with thermal Kaolite as well. The heat loss value was also considered in the uncertainty analysis to ensure that the reported values for the heat transfer coefficient were accurate.

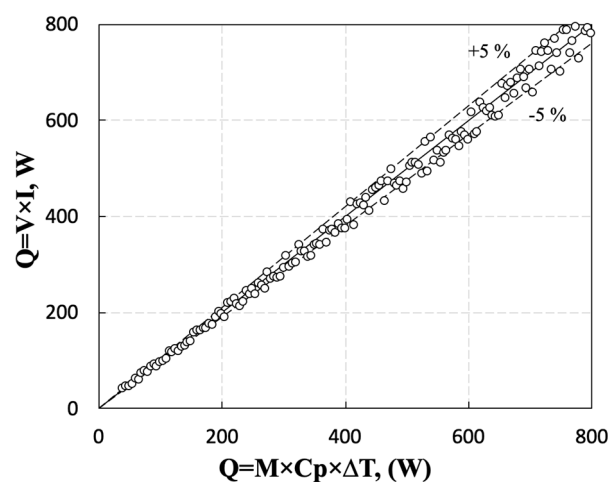


Figure 2. Heat loss analysis conducted on the test section of the test facility.

The roughness of the surface is an important variable, especially at the test section, because it affects the rate of the bubble formation and the heat transfer coefficient value. It has already been demonstrated that the surface roughness must be uniform in order to create a uniform temperature distribution on the bubble generation surface [55–60]. Hence, a profilometer was employed to quantify the variation of the surface roughness with the length of the surface. Based on Figure 3, surface roughness varies around $1 \mu\text{m} \pm 0.2 \mu\text{m}$. Also, the regression analysis revealed that $>85\%$ of the measured points have a roughness value of $\sim 1 \mu\text{m}$. Likewise, scanning electron microscopy was used to report the surface morphology as well. As can be seen in Figure 3, the surface morphology is uniform and the irregularities and micro-cavities have been distributed uniformly on the boiling surface. Hence, the bubble formation induced by the surface roughness is weak, and the generation of the bubbles via heat flux is the dominant mechanism of bubble formation over the surface.

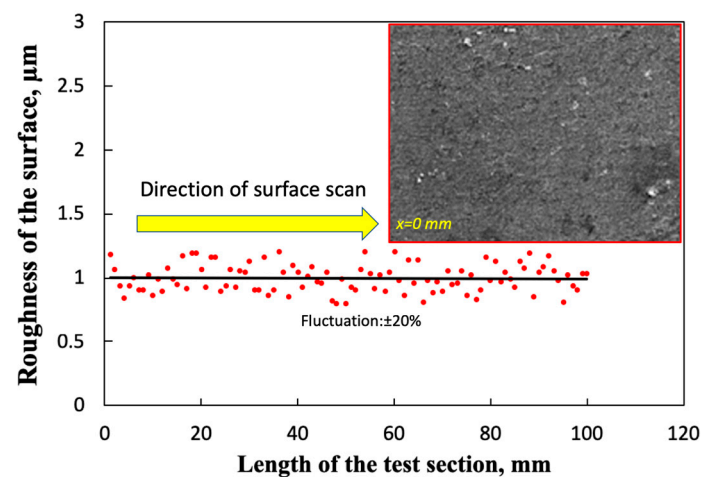


Figure 3. Plot of surface roughness vs. test section length (at the area where the bubble are formed). Inset: Scanning electron microscopy taken from the initial section of the surface.

Kline-McClintock's method was used for uncertainty analysis [61]. Considering the accuracy of the instruments—including ± 1 K for thermocouples, $\pm 1\%$ for flow rate, 1 pixel for image processing, 0.5% for RTD thermometer, 0.1% for voltage, and 1% for current (accuracy of multi-meter is different for voltage and current)—it was identified that the uncertainty value for the heat transfer coefficient is 5.1%, for contact angle 5%, and for heat flux 4%, respectively. The uncertainty value includes the heat loss analysis and repeatability of the experiments.

3. Results

Figure 4 represents the typical boiling curve for water at atmospheric pressure and various heat transfer regimes. As can be seen, various operating regimes can be identified from the boiling curve of water. The first regime, in which the temperature difference between surface and the liquid is ~ 5 K, is referred to as the “forced convective regime”, in which still bubbles are not formed on the surface and as a result, the heat transfer coefficient is relatively small. By increasing the surface temperature, the temperature difference reaches ~ 10 K. In this region, the first bubbles form on the surface, resulting in a significant increase in the heat transfer coefficient of the system, and the “nucleate boiling regime” forms. By increasing the surface temperature, the temperature difference (superheat degree) reaches ~ 30 K, in which critical heat flux (CHF) occurs [62]. In the CHF point, the bubble formation rate is intensified such that the bubbles are merged and create a vapor blanket covering the surface, and the heat transfer coefficient decreases. From this point, by increasing the temperature difference, instability increases on the surface, resulting in the decrease in heat transfer rate from the surface towards the liquid, creating to the region called “film boiling”. The boundary between the film boiling and the transient boiling regions is referred to as “minimum stable film boiling” point. From this point, the vapor production is not strong enough to keep liquid away from the surface. By re-contacting the liquid with the boiling surface, the efficient heat transfer resumes and again heat transfer is promoted [63]. In the present work, we were looking into the forced convective and nucleate boiling heat transfer regime in which the temperature difference between surface and the liquid (superheat degree) is less than 30 K [62].

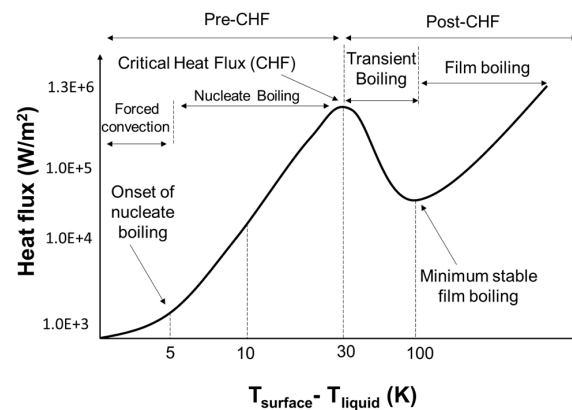


Figure 4. The boiling curve for water at atmospheric pressure.

3.1. HTC or Heat Transfer Coefficient

Figure 5 shows heat transfer coefficient vs. thermal flux for mass flow rate of 1 L/min and 50 °C temperature at the inlet. As can be seen, the HTC shows different behavior depending on the value of the heat flux (HF). For HFs <15 kW/m², the dominant mechanism of the heat transfer between the water and the stainless steel rod is “forced convective heat transfer”; however, for larger HFs (e.g., >15 kW/m²), the HTC dramatically increases, which is largely due to the formation of the bubbles on the surface. Bubbles absorb the thermal energy in the form of sensible and latent heat from the boiling micro-layer, and transfer it in the form of water vapor to the bulk of the water. Hence, the surface can transfer a large amount of heat to the bulk of the fluid in comparison with the single-phase heat transfer. It is worth saying that, at a low HF region, as can be seen from the figure, the bubbles can be distinguished; however, for a high HF region, the column of bubbles form close to the surface. As a result, there is a high heat transfer from the surface. Consequently, a higher HF results in a higher HTC. For instance, HF = 10 kW/m² corresponds to HTC = ~1870 W/(m²K), and for HF = 90 kW/m², HTC = ~9000 W/(m²K). Interestingly, the presence of the total dissolved solid materials within the bulk of the water influences the thermal conductivity and boiling-related sub-phenomena within the water. The more the TDS value of particles, the larger the thermal conductivity and the Brownian motion of the TDS particles within water. Brownian motion can potentially intensify the thermal transport and heat transfer within the liquid [64]. The TDS materials can receive the surface heat and convey it to the cold regions by Brownian motion of the particles. Hence, the larger the TDS concentration, the higher the HTC. For instance, the HTC was 8040 W/(m²K), 8610 W/(m²K), and ~9000 W/(m²K) at the TDS values of 300 mg/L, 750 mg/L, and 1200 mg/L, respectively (for HF = 90 kW/m²), which was attributed to the enhancement in thermo-physical properties of water [65].

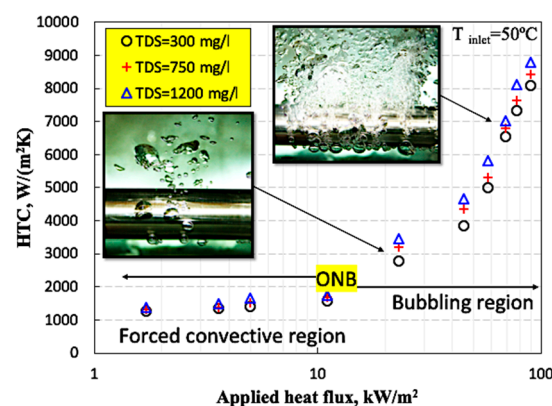


Figure 5. Heat transfer rate vs. thermal flux for different total dissolved solid materials (TDS) values and bubble formation as a function of heat flux at TDS = 300 mg/L.

3.2. Bubble Diameter

Figure 6 represents the effect of the heat flux on bubble formation at an inlet temperature of 90 °C, close to the saturation temperature of water and at a TDS value of 1200 mg/L. Increasing the value of surface HF results in a higher bubble formation rate. However, the increase influences the size of the bubbles such that at large HF values, the bubbles are merged to form bigger bubbles. Also, at larger HFs as shown in Figure 6, the bubble jets are formed, which intensify the heat transfer rate from the surface. It is worth saying that the formation of the bubble columns creates micro-streams of fluid around the heating section, which can further improve the cooling performance of the system. Hence, a trade-off is identified between the size of the bubbles and the rate of the heat transfer. For larger HFs, the bubbles are merged, creating bigger bubbles, which in turn cover the heating surface. Since bubbles contain water vapor, the thermal conductivity of vapor is smaller than that measured for liquids, and as a result, the boiling surface is covered with insulation-like vapor. Thus, it is expected that the HTC of water decreases; however, due to the formation of the bubble column and increase in the frequency of bubble generation, the bigger bubbles quickly depart the surface and provide opportunity for the young ones to form and absorb the heat from the surface. Thus, despite the increase in the average bubble diameter at large heat flux values, the thermal performance of the system is improved.

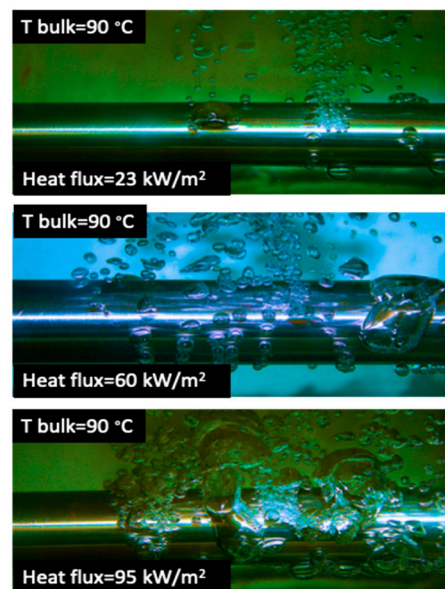


Figure 6. Visualization of the bubble formation inside the annulus pipe at various heat fluxes and for water with TDS value of 1200 mg/L.

Despite plausible characteristics of bubble formation in heat transfer systems, particularly in pool and flow boiling heat transfer regimes, the presence of bubbles can induce some disadvantages in the system. The formation of bubbles can create a massive wear in engineering systems and cavities where the operating pressure of the system or the cavity is relatively low. The collapse of bubbles close or on the metallic surface can cause cyclic stress, which creates fatigue due to a process called cavitation. Also, in pumps and loops, the presence of bubbles can add corrosion to the casing and the joints. When it comes to heat transfer surfaces in confined space (e.g., CPU cooling systems or compact heat exchangers), an increase in bubble formation can partially cover the surface and act as surface insulation, decreasing the heat transfer from the surface towards the bulk of the liquids. The turbulence, due to the bubble interactions with surface and liquid at a high Reynolds number, can also create micro-tension forces, which add to the corrosion of the materials. Hence, further study on disadvantage of the bubbles in the system is highly recommended, which is beyond the scope of the present research.

3.3. Contact Angle

Figure 7 shows the effect of the TDS value of water on the contact angle of the vapor surface. As can be seen, for water with a TDS value of 300 mg/L, the size of the bubble is smaller and the contact angle formed on the surface is also smaller than that reported for water with larger TDS values. For example, at a TDS value of 1200 mg/L, the contact angle reaches 124° and the bubble lies completely down on the surface. Hence, more surface contact is available between the bubble and the boiling surface and, as a result, more heat transfer rate occurs between the heating surface and the bubbles. Hence, increasing the mass concentration of the TDS materials within the water can potentially improve the thermal properties, contact angle, and bubble diameter such that with an increase in the TDS value, the larger bubbles form with larger contact angles and diameters, causing better thermal performance in the system. Notably, there is a limit for TDS values because from a certain value (here, more than 1300 mg/L), a layer of TDS is deposited on the surface, which can change the roughness of the surface, causing a thermal resistance, which decreases the frequency of bubble formation. Notably, the study on the effect of TDS deposition is not within the reach of the current work.

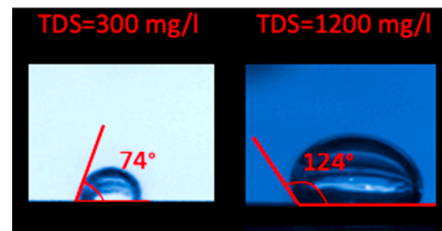


Figure 7. Contact angle measurements for water at TDS values of (left) 300 mg/L and (right) 1200 mg/L at heat flux of 50 kW/m^2 .

3.4. Comparison Against the Developed Models

Figure 8 shows the variation of the measured bubble diameter with the TDS of water and a comparison between the bubble diameter estimated with Fritz [66] and Cole [67] equations for 50 kW/m^2 thermal flux. By increasing the TDS value of water, the average bubble diameter increases. For example, at a TDS value of 300 mg/L, a bubble diameter of 0.0041 m to 0.0046 m was reported; however, for a TDS value of 1200 mg/L, the bubble diameter increased to 0.0068 m to 0.0088 m. As can be seen, the variation in the bubble diameter size is a strong function of the TDS value such that the range of the bubble diameter for water with a TDS value of 1200 mg/L is wider than that observed for water at a TDS value of 300 mg/L. This is because TDS materials change the water properties. However, studying these attributes is beyond the scope of the current study. The results from the Fritz and Cole formula were compared with the experimental results as well.

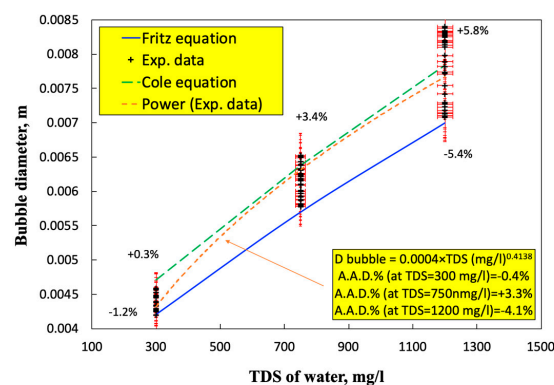


Figure 8. Dependence of the bubble diameter on the TDS value, and a comparison between the results calculated with Fritz and Cole equations against experimental data.

As can be seen, the experimental data are in a good agreement with the calculated results, showing the reasonable accuracy and reliability of the measurement technique. The absolute average deviation of the Fritz and Cole equations for predicting the bubble diameter at various TDS values was $\pm 1.2\%$, $\pm 3.4\%$, and $\pm 5.8\%$ for TDS values of 300, 750, and 1200 mg/L, respectively, and the experimental bubble diameter values were distributed within the region captured by these two equations. Since a semi-linear behavior was identified between bubble diameter and the TDS value, a simple regression analysis was employed to correlate the bubble diameter to the TDS value, which can estimate the bubble diameter with more accuracy.

3.5. Flow Rate of Water

Figure 9 shows the effect of the flow rate of the water on the bubble formation inside the annulus pipe at heat flux of 50 kW/m^2 for various flow rates. Increasing the water's mass flow rate around the stainless steel rod results in suppression of the bubble formation around the heating section, as shown in Figure 8. At a flow rate of 5 L/min, the bubbles are very small and can barely be identified. However, with a decrease in the flow rate (Q), e.g., from 5 L/min to 3 L/min, the bubble formation becomes immensely strong and the bubbles become clearly visible around the surface of the rod. For $Q = 1 \text{ L/min}$, high amounts of bubbles are generated and it is close to the formation of the bubble jets. This is because, when the flow rate of water is small, the micro-layer close to the surface has sufficient residence time and diffusion of the vapor from this micro-layer to the bubbles is a strong mechanism affecting the bubble size. However, by increasing the fluid flow, regeneration of the micro-layer in proximity to the surface occurs swiftly, and the diffusion mechanism becomes weak, while the convective mechanism is the dominant mechanism of heat transfer around the surface. Therefore, flow rate is a key operating parameter controlling the bubble growth and the average size of the bubbles around the surface.

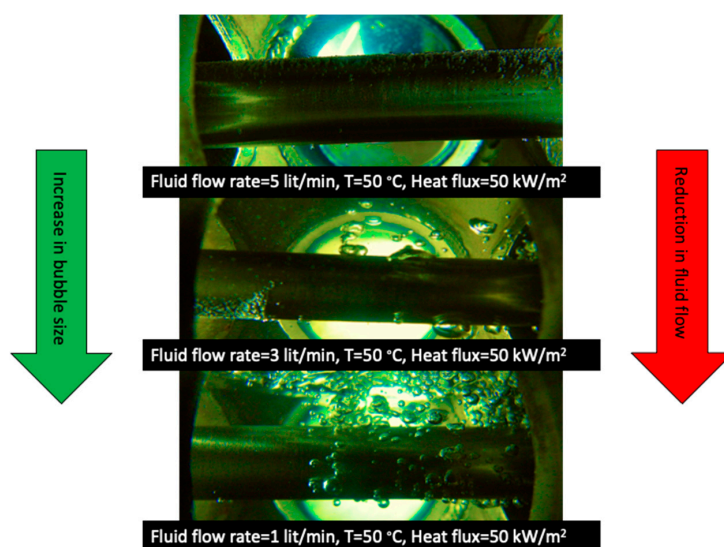


Figure 9. The effect of the fluid flow rate on the average bubble diameter and bubble formation rate on the heating surface at $50 \text{ }^{\circ}\text{C}$.

Figure 10 shows the variation of HTC vs. Q for thermal flux equal to 75 kW/m^2 for various TDS values of water. Increasing Q results in higher HTC; for example, for water with a TDS value of 300 mg/L, for $Q = 1 \text{ L/min}$, $\text{HTC} = \sim 5000 \text{ W/(m}^2\text{K)}$, and at $Q = 8 \text{ L/min}$, $\text{HTC} = 6800 \text{ W/(m}^2\text{K)}$. Higher TDS of water results in the rise of the HTC value of the system. The largest HTC was recorded at the highest flow rate of 8 L/min and a TDS value of 1200 mg/L. This can be attributed to the formation of larger bubbles, improvement in the thermal conductivity of the water, and the increase in the contact angle, which in turn increases the contact between the bubble and the surface.

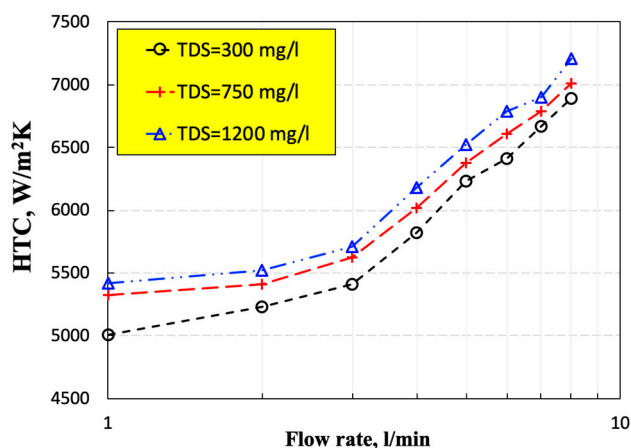


Figure 10. Curves of heat transfer coefficient (HTC) vs. flow rate (Q) for different TDS values at thermal flux equal to 75 kW/m^2 .

3.6. Chemical Composition and Thermal Conductivity Measurement

Figure 11 presents the variation of the thermal conductivity of the water, with concentrations of TDS materials in the water. As can be seen, the thermal conductivity of the water increases with an increase in the concentration of TDS materials. Here, a TDS value of 200 mg/L was considered as a reference case. As can be seen, at a TDS value of 300 mg/L , the thermal conductivity enhancement is 0.5% , while at 1000 and 1200 mg/L , it reaches 2.4% and 3.2% , respectively, which of course results in the improvement of the heat transfer rate of the system. Also, the presence of the TDS material can increase the Brownian motion phenomenon [68,69] which intensifies the heat transfer coefficient as well. For better understanding, the chemical composition of the water used in the present research has been presented in Table 1.

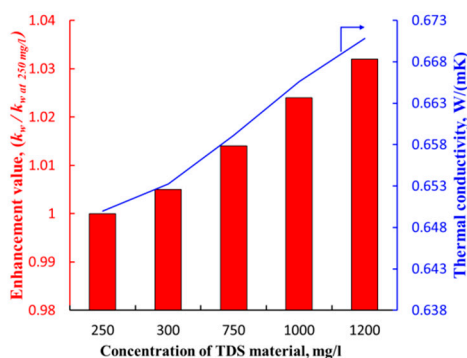


Figure 11. Variation of the enhancement of thermal conductivity with concentration of TDS material.

It is worth saying that the presence of ions such as sodium and calcium can improve the electrical conductivity of the water, and some materials—such as K—can improve the thermal conductivity of water. Table 2 shows the chemical composition of water used in the present research.

Table 2. Chemical composition of water used in the present research.

Parameter	Value	Unit
Electrical conductivity at TDS = 250 mg/L	0.651	W/(mK)
pH	7.05	-
Na ⁺	140	mg/L
Ca ²⁺	95	mg/L
Mg ²⁺	29.8	mg/L
K ⁺	5.1	mg/L
F ⁻	0.11	mg/L

4. Conclusions

In the present work, an experimental investigation was conducted on the convective bubbly flow of water in an annulus pipe, with the aim of evaluating the bubble intensity of the heat transfer coefficient of water fluid at various TDS values. The following conclusions were made:

- (1) It was identified that the presence of total dissolved solid materials can improve the thermal conductivity of water, and plausibly influences the bubble formation characteristics of the system. Results show that the thermal conductivity of water can be improved by ~3.2% when the TDS materials increased from 250 mg/L to 1200 mg/L.
- (2) Increasing the TDS mass fraction resulted in larger bubble diameters, the contact angle between the bubble and the heating surface increased, and the heat transfer coefficient of the system was enlarged. It was also identified that the flow rate of water can considerably change the bubble diameter size, such that for $Q = 5$ L/min, suppression of bubble formation occurred at subcooled regime. Hence, bubbles were larger at low flow rates, e.g., 1 L/min. The highest heat transfer coefficient of >9000 W/(m²K) was reported for water with a TDS value of 1200 mg/L at flow rate of 8 L/min, despite the reduction in the bubble size, as the thermal boundary layer was renewed quickly.
- (3) Forced convective heat transfer and nucleate boiling were the dominant mechanisms of heat transfer in the system, which were separated with a point referred to as onset of nucleate boiling, in which the first bubbles form on the surface. Thereby, the presence of TDS materials in water can promote the bubble formation, resulting in the enhancement of the mixing and heat transfer coefficient.
- (4) Overall, the bubble formation—despite its plausible heat transfer characteristics—can have some disadvantages, such as cavitation, corrosion, and wear, which need further study. Especially for the metallic pipes, wear can induce a massive corrosion to the system over time. A comprehensive study in this area is highly recommended. Also, the influence of TDS on physical properties of water should be studied, along with its effect on the boiling mechanism. Studying these topics can broaden the knowledge of two-phase heat transfer.

Author Contributions: Conceptualization, M.M.S., M.S.S., and M.R.S.; methodology, M.S.S., M.R.S., and M.M.S.; formal analysis, M.M.S., M.G., M.A., and M.S.S.; investigation, M.M.S., M.G., M.A., I.T., T.A.A., Z.T., and M.S.S.; writing—original draft preparation, M.M.S., M.G., M.S.S., M.A., Z.T., I.T., and T.A.A.; writing—review and editing, M.A.; visualization, M.S.S., M.A., and M.M.S.; and supervision, M.A.

Funding: This research received no external funding.

Acknowledgments: The first author of this work acknowledges Peyghambarzadeh and Alavi Fazel for their scientific support during the experiments conducted in IAU in 2014. Zhe Tian wants to acknowledge the following grants: NSFC (51709244), Taishan Scholar (tsqn201812025), and Fundamental Research for Central Universities (201941008). Last but not least, the authors extend their appreciation to the Deanship of Scientific Research at Majmaah University for funding this work under project number No. (RGP-2019-17).

Conflicts of Interest: The authors declare no conflict of interest.

References

1. Bergles, A.E.; Collier, J.; Delhay, J.M.; Hewitt, G.; Mayinger, F. *Two-Phase Flow and Heat Transfer in the Power and Process Industries*; Hemisphere Publishing Corp.: New York, NY, USA, 1981.
2. Saha, K.; Agarwal, A.K.; Ghosh, K.; Som, S. (Eds.) *Two-Phase Flow for Automotive and Power Generation Sectors*; Springer: Singapore, 2019.
3. Kandlikar, S.G. *Handbook of Phase Change: Boiling and Condensation*; Routledge: Abingdon-on-Thames, UK, 2018.
4. Marcinichen, J.B.; Thome, J.R.; Michel, B. Cooling of microprocessors with micro-evaporation: A novel two-phase cooling cycle. *Int. J. Refrig.* **2010**, *33*, 1264–1276. [[CrossRef](#)]
5. Cengel, Y. *Heat and Mass Transfer: Fundamentals and Applications*; McGraw-Hill: USA, 2014.
6. Murshed, S.S.; De Castro, C.N. A critical review of traditional and emerging techniques and fluids for electronics cooling. *Renew. Sustain. Energy Rev.* **2017**, *78*, 821–833. [[CrossRef](#)]
7. Storm, K. Chapter 4—Waste heat boiler. In *Industrial Process Plant Construction Estimating and Man-Hour Analysis*; Storm, K., Ed.; Gulf Professional Publishing: Oxford, UK, 2019; pp. 67–78.
8. Park, K.-J.; Jung, D. Boiling heat transfer enhancement with carbon nanotubes for refrigerants used in building air-conditioning. *Energy Build.* **2007**, *39*, 1061–1064. [[CrossRef](#)]
9. Ding, W.; Zhang, P.; Li, Y.; Xia, H.; Wang, D.; Tao, X. Effect of latent heat in boiling water on the synthesis of gold nanoparticles of different sizes by using the turkevich method. *ChemPhysChem* **2015**, *16*, 447–454. [[CrossRef](#)] [[PubMed](#)]
10. Moita, A.; Teodori, E.; Moreira, A. Influence of surface topography in the boiling mechanisms. *Int. J. Heat Fluid Flow* **2015**, *52*, 50–63. [[CrossRef](#)]
11. Magnini, M.; Thome, J. A cfd study of the parameters influencing heat transfer in microchannel slug flow boiling. *Int. J. Therm. Sci.* **2016**, *110*, 119–136. [[CrossRef](#)]
12. Piasecka, M. Impact of selected parameters on refrigerant flow boiling heat transfer and pressure drop in minichannels. *Int. J. Refrig.* **2015**, *56*, 198–212. [[CrossRef](#)]
13. Pothukuchi, H.; Kelm, S.; Patnaik, B.; Prasad, B.; Allelein, H.-J. Numerical investigation of subcooled flow boiling in an annulus under the influence of eccentricity. *Appl. Therm. Eng.* **2018**, *129*, 1604–1617. [[CrossRef](#)]
14. Guo, D.; Sun, D.; Li, Z.; Tao, W. Phase change heat transfer simulation for boiling bubbles arising from a vapor film by the voset method. *Numer. Heat Transf. Part A Appl.* **2011**, *59*, 857–881. [[CrossRef](#)]
15. Forster, H.; Zuber, N. Dynamics of vapor bubbles and boiling heat transfer. *AIChE J.* **1955**, *1*, 531–535. [[CrossRef](#)]
16. Lu, M.-C.; Tong, J.-R.; Wang, C.-C. Investigation of the two-phase convective boiling of hfo-1234yf in a 3.9 mm diameter tube. *Int. J. Heat Mass Transf.* **2013**, *65*, 545–551. [[CrossRef](#)]
17. Yan, J.; Bi, Q.; Liu, Z.; Zhu, G.; Cai, L. Subcooled flow boiling heat transfer of water in a circular tube under high heat fluxes and high mass fluxes. *Fusion Eng. Des.* **2015**, *100*, 406–418. [[CrossRef](#)]
18. Kim, J. Review of nucleate pool boiling bubble heat transfer mechanisms. *Int. J. Multiph. Flow* **2009**, *35*, 1067–1076. [[CrossRef](#)]
19. Jung, S.; Kim, H. An experimental method to simultaneously measure the dynamics and heat transfer associated with a single bubble during nucleate boiling on a horizontal surface. *Int. J. Heat Mass Transf.* **2014**, *73*, 365–375. [[CrossRef](#)]
20. Pan, L.-M.; Tan, Z.-W.; Chen, D.-Q.; Xue, L.-C. Numerical investigation of vapor bubble condensation characteristics of subcooled flow boiling in vertical rectangular channel. *Nucl. Eng. Des.* **2012**, *248*, 126–136. [[CrossRef](#)]
21. Julia, J.E.; Hibiki, T. Flow regime transition criteria for two-phase flow in a vertical annulus. *Int. J. Heat Fluid Flow* **2011**, *32*, 993–1004. [[CrossRef](#)]
22. Hernández, L.; Julia, J.E.; Ozar, B.; Hibiki, T.; Ishii, M. Flow regime identification in boiling two-phase flow in a vertical annulus. *J. Fluids Eng.* **2011**, *133*, 091304. [[CrossRef](#)]
23. Kandlikar, S.G. A general correlation for saturated two-phase flow boiling heat transfer inside horizontal and vertical tubes. *J. Heat Transf.* **1990**, *112*, 219–228. [[CrossRef](#)]
24. Sarafraz, M.M.; Peyghambarzadeh, S.M.; Vaeli, N. Subcooled flow boiling heat transfer of ethanol aqueous solutions in vertical annulus space. *Chem. Ind. Chem. Eng. Q.* **2012**, *18*, 315–327. [[CrossRef](#)]
25. Brooks, C.S.; Ozar, B.; Hibiki, T.; Ishii, M. Interfacial area transport of subcooled boiling flow in a vertical annulus. *Nucl. Eng. Des.* **2014**, *268*, 152–163. [[CrossRef](#)]
26. Sadeghi, R.; Shadloo, M.S.; Hooman, K. Numerical investigation of the natural convection film boiling around elliptical tubes. *Numer. Heat Transf. Part A Appl.* **2016**, *70*, 707–722. [[CrossRef](#)]

27. Lahey, R., Jr.; Ohkawa, K. An experimental investigation of phase distribution in an eccentric annulus. *Int. J. Multiph. Flow* **1989**, *15*, 447–457. [\[CrossRef\]](#)
28. Kelessidis, V.; Dukler, A. Modeling flow pattern transitions for upward gas-liquid flow in vertical concentric and eccentric annuli. *Int. J. Multiph. Flow* **1989**, *15*, 173–191. [\[CrossRef\]](#)
29. Osamusali, S.; Chang, J. Two-phase flow regime transition in a horizontal pipe and annulus flow under gas-liquid two-phase flow. *ASME Fed.* **1988**, *72*, 63–69.
30. Ekberg, N.; Ghiaasiaan, S.; Abdel-Khalik, S.; Yoda, M.; Jeter, S. Gas-liquid two-phase flow in narrow horizontal annuli. *Nucl. Eng. Des.* **1999**, *192*, 59–80. [\[CrossRef\]](#)
31. Thorncroft, G.E.; Klausner, J.F.; Mei, R. An experimental investigation of bubble growth and detachment in vertical upflow and downflow boiling. *Int. J. Heat Mass Transf.* **1998**, *41*, 3857–3871. [\[CrossRef\]](#)
32. Bibeau, E.L.; Salcudean, M. A study of bubble ebullition in forced-convective subcooled nucleate boiling at low pressure. *Int. J. Heat Mass Transf.* **1994**, *37*, 2245–2259. [\[CrossRef\]](#)
33. Situ, R.; Hibiki, T.; Ishii, M.; Mori, M. Bubble lift-off size in forced convective subcooled boiling flow. *Int. J. Heat Mass Transf.* **2005**, *48*, 5536–5548. [\[CrossRef\]](#)
34. Chen, C.A.; Chang, W.R.; Li, K.W.; Lie, Y.M.; Lin, T.F. Subcooled flow boiling heat transfer of r-407c and associated bubble characteristics in a narrow annular duct. *Int. J. Heat Mass Transf.* **2009**, *52*, 3147–3158. [\[CrossRef\]](#)
35. Gerardi, C.; Buongiorno, J.; Hu, L.-W.; McKrell, T. Study of bubble growth in water pool boiling through synchronized, infrared thermometry and high-speed video. *Int. J. Heat Mass Transf.* **2010**, *53*, 4185–4192. [\[CrossRef\]](#)
36. Sugrue, R.; Buongiorno, J.; McKrell, T. An experimental study of bubble departure diameter in subcooled flow boiling including the effects of orientation angle, subcooling, mass flux, heat flux, and pressure. *Nucl. Eng. Des.* **2014**, *279*, 182–188. [\[CrossRef\]](#)
37. Lazarek, G.M.; Black, S.H. Evaporative heat transfer, pressure drop and critical heat flux in a small vertical tube with r-113. *Int. J. Heat Mass Transf.* **1982**, *25*, 945–960. [\[CrossRef\]](#)
38. Jung, D.S.; McLinden, M.; Radermacher, R.; Didion, D. Horizontal flow boiling heat transfer experiments with a mixture of r22/r114. *Int. J. Heat Mass Transf.* **1989**, *32*, 131–145. [\[CrossRef\]](#)
39. Bao, Z.; Fletcher, D.; Haynes, B. Flow boiling heat transfer of freon r11 and hfc123 in narrow passages. *Int. J. Heat Mass Transf.* **2000**, *43*, 3347–3358. [\[CrossRef\]](#)
40. Yeoh, G.H.; Tu, J.Y. A unified model considering force balances for departing vapour bubbles and population balance in subcooled boiling flow. *Nucl. Eng. Des.* **2005**, *235*, 1251–1265. [\[CrossRef\]](#)
41. Chang, Y.; Ferng, Y. Experimental investigation on bubble dynamics and boiling heat transfer for saturated pool boiling and comparison data with previous works. *Appl. Therm. Eng.* **2019**, *154*, 284–293. [\[CrossRef\]](#)
42. Wang, J.; Cheng, Y.; Li, X.-B.; Li, F.-C. Experimental and lbm simulation study on the effect of bubbles merging on flow boiling. *Int. J. Heat Mass Transf.* **2019**, *132*, 1053–1061. [\[CrossRef\]](#)
43. Yin, X.; Tian, Y.; Zhou, D.; Wang, N. Numerical study of flow boiling in an intermediate-scale vertical tube under low heat flux. *Appl. Therm. Eng.* **2019**, *153*, 739–747. [\[CrossRef\]](#)
44. Eraghubi, M.; Di Marco, P.; Robinson, A. Low mass flux upward vertical forced flow boiling of hfe7000. *Exp. Therm. Fluid Sci.* **2019**, *102*, 291–301. [\[CrossRef\]](#)
45. Suleman, M.; Ramzan, M.; Ahmad, S.; Lu, D.; Muhammad, T.; Chung, J.D. A numerical simulation of silver-water nanofluid flow with impacts of newtonian heating and homogeneous-heterogeneous reactions past a nonlinear stretched cylinder. *Symmetry* **2019**, *11*, 295. [\[CrossRef\]](#)
46. Saif, R.S.; Hayat, T.; Ellahi, R.; Muhammad, T.; Alsaedi, A. Darcy-forchheimer flow of nanofluid due to a curved stretching surface. *Int. J. Numer. Methods Heat Fluid Flow* **2019**, *29*, 2–20. [\[CrossRef\]](#)
47. Sarafraz, M.M.; Arjomandi, M. Contact angle and heat transfer characteristics of a gravity-driven film flow of a particulate liquid metal on smooth and rough surfaces. *Appl. Therm. Eng.* **2019**, *149*, 602–612. [\[CrossRef\]](#)
48. Peyghambarzadeh, S.M.; Sarafraz, M.M.; Vaeli, N.; Ameri, E.; Vatani, A.; Jamialahmadi, M. Forced convective and subcooled flow boiling heat transfer to pure water and n-heptane in an annular heat exchanger. *Ann. Nucl. Energy* **2013**, *53*, 401–410. [\[CrossRef\]](#)
49. Sarafraz, M.M.; Arya, H.; Saeedi, M.; Ahmadi, D. Flow boiling heat transfer to mgo-therminol 66 heat transfer fluid: Experimental assessment and correlation development. *Appl. Therm. Eng.* **2018**, *138*, 552–562. [\[CrossRef\]](#)

50. Sarafraz, M.M.; Hormozi, F. Scale formation and subcooled flow boiling heat transfer of cuo–water nanofluid inside the vertical annulus. *Exp. Therm. Fluid Sci.* **2014**, *52*, 205–214. [[CrossRef](#)]
51. Sarafraz, M.M.; Hormozi, F. Forced convective and nucleate flow boiling heat transfer to alumina nanofluids. *Period. Polytech. Chem. Eng.* **2014**, *58*, 37–46. [[CrossRef](#)]
52. Sarafraz, M.M.; Hormozi, F.; Peyghambarzadeh, S.M.; Vaeli, N. Upward flow boiling to di-water and cuo nanofluids inside the concentric annuli. *J. Appl. Fluid Mech.* **2015**, *8*, 651–659.
53. Goshayeshi, H.R.; Goodarzi, M.; Safaei, M.R.; Dahari, M. Experimental study on the effect of inclination angle on heat transfer enhancement of a ferrofluid in a closed loop oscillating heat pipe under magnetic field. *Exp. Therm Fluid Sci.* **2016**, *74*, 265–270. [[CrossRef](#)]
54. Sarafraz, M.M.; Peyghambarzadeh, S.M. Experimental study on subcooled flow boiling heat transfer to water–diethylene glycol mixtures as a coolant inside a vertical annulus. *Exp. Therm. Fluid Sci.* **2013**, *50*, 154–162. [[CrossRef](#)]
55. Nikkhah, V.; Sarafraz, M.M.; Hormozi, F. Application of spherical copper oxide (ii) water nano-fluid as a potential coolant in a boiling annular heat exchanger. *Chem. Biochem. Eng. Q.* **2015**, *29*, 405–415. [[CrossRef](#)]
56. Salari, E.; Peyghambarzadeh, M.; Sarafraz, M.M.; Hormozi, F. Boiling heat transfer of alumina nano-fluids: Role of nanoparticle deposition on the boiling heat transfer coefficient. *Period. Polytech. Chem. Eng.* **2016**, *60*, 252–258. [[CrossRef](#)]
57. Salari, E.; Peyghambarzadeh, S.M.; Sarafraz, M.M.; Hormozi, F.; Nikkhah, V. Thermal behavior of aqueous iron oxide nano-fluid as a coolant on a flat disc heater under the pool boiling condition. *Heat Mass Transf.* **2017**, *53*, 265–275. [[CrossRef](#)]
58. Sarafraz, M.M. Nucleate pool boiling of aqueous solution of citric acid on a smoothed horizontal cylinder. *Heat Mass Transf.* **2012**, *48*, 611–619. [[CrossRef](#)]
59. Sarafraz, M.M. Experimental investigation on pool boiling heat transfer to formic acid, propanol and 2-butanol pure liquids under the atmospheric pressure. *J. Appl. Fluid Mech.* **2013**, *6*, 73–79.
60. Sarafraz, M.M.; Peyghambarzadeh, S.M. Influence of thermodynamic models on the prediction of pool boiling heat transfer coefficient of dilute binary mixtures. *Int. Commun. Heat Mass Transf.* **2012**, *39*, 1303–1310. [[CrossRef](#)]
61. Kline, S.J. Describing uncertainties in single-sample experiments. *Mech. Eng.* **1953**, *75*, 3–8.
62. Butterworth, D.; Hewitt, G.F. (Eds.) *Two-Phase Flow and Heat Transfer*; Oxford University Press: Oxford, UK, 1977; 514p.
63. Sadeghi, R.; Shadloo, M.S. Three-dimensional numerical investigation of film boiling by the lattice boltzmann method. *Numer. Heat Transf. Part A Appl.* **2017**, *71*, 560–574. [[CrossRef](#)]
64. Malvandi, A.; Heysiattalab, S.; Ganji, D.D. Thermophoresis and brownian motion effects on heat transfer enhancement at film boiling of nanofluids over a vertical cylinder. *J. Mol. Liq.* **2016**, *216*, 503–509. [[CrossRef](#)]
65. Sadeghi, R.; Shadloo, M.S.; Jamalabadi, M.Y.A.; Karimipour, A. A three-dimensional lattice boltzmann model for numerical investigation of bubble growth in pool boiling. *Int. Commun. Heat Mass Transf.* **2016**, *79*, 58–66. [[CrossRef](#)]
66. Jensen, M.K.; Memmel, G.J. Evaluation of bubble departure diameter correlations. In Proceedings of the 8th International Heat Transfer Conference, San Francisco, CA, USA, 17–22 August 1986; pp. 1907–1912.
67. Cole, R.; Rohsenow, W.M. Correlation of bubble departure diameters for boiling of saturated liquids. *Chem. Eng. Prog. Symp. Ser.* **1969**, *65*, 211–213.
68. Hayat, T.; Muhammad, T.; Shehzad, S.A.; Alsaedi, A. An analytical solution for magnetohydrodynamic oldroyd-b nanofluid flow induced by a stretching sheet with heat generation/absorption. *Int. J. Therm. Sci.* **2017**, *111*, 274–288. [[CrossRef](#)]
69. Mahanthesh, B.; Gireesha, B.J.; Animasaun, I.L.; Muhammad, T.; Shashikumar, N.S. Mhd flow of swcnt and mwcnt nanoliquids past a rotating stretchable disk with thermal and exponential space dependent heat source. *Phys. Scr.* **2019**, *94*, 085214. [[CrossRef](#)]

